



UNIVERSITY OF LEEDS

This is a repository copy of *Reutilization of fluid flow pathways over 54 million years, offshore New Zealand*.

White Rose Research Online URL for this paper:

<https://eprints.whiterose.ac.uk/200878/>

Version: Accepted Version

Article:

Cao, L, Sun, Q and Magee, C orcid.org/0000-0001-9836-2365 (Cover date: December 2023) *Reutilization of fluid flow pathways over 54 million years, offshore New Zealand*. *Basin Research*, 35 (6). pp. 2349-2363. ISSN 0950-091X

<https://doi.org/10.1111/bre.12801>

© 2023 International Association of Sedimentologists and European Association of Geoscientists and Engineers and John Wiley & Sons Ltd. This is the peer reviewed version of the following article: Cao, L, Sun, Q and Magee, C (2023) *Reutilization of fluid flow pathways over 54 million years, offshore New Zealand*. *Basin Research*. ISSN 0950-091X, which has been published in final form at <https://doi.org/10.1111/bre.12801>. This article may be used for non-commercial purposes in accordance with Wiley Terms and Conditions for Use of Self-Archived Versions. This article may not be enhanced, enriched or otherwise transformed into a derivative work, without express permission from Wiley or by statutory rights under applicable legislation. Copyright notices must not be removed, obscured or modified. The article must be linked to Wiley's version of record on Wiley Online Library and any embedding, framing or otherwise making available the article or pages thereof by third parties from platforms, services and websites other than Wiley Online Library must be prohibited.

Reuse

Items deposited in White Rose Research Online are protected by copyright, with all rights reserved unless indicated otherwise. They may be downloaded and/or printed for private study, or other acts as permitted by national copyright laws. The publisher or other rights holders may allow further reproduction and re-use of the full text version. This is indicated by the licence information on the White Rose Research Online record for the item.

Takedown

If you consider content in White Rose Research Online to be in breach of UK law, please notify us by emailing eprints@whiterose.ac.uk including the URL of the record and the reason for the withdrawal request.



eprints@whiterose.ac.uk
<https://eprints.whiterose.ac.uk/>

1 **Reutilization of hydrothermal fluid flow pathways over 54 million years, offshore**
2 **New Zealand**

3 **Liu Cao¹, Qiliang Sun^{1,2*}, Craig Magee³**

4 ¹Key Laboratory of Tectonics and Petroleum Resources, China University of Geosciences
5 (Wuhan), Ministry of Education, Wuhan 430074, China

6 ²Laboratory for Marine Mineral Resources, Qingdao National Laboratory for Marine Science
7 and Technology, Qingdao 266061, China

8 ³Institute of Geophysics and Tectonics, School of Earth Science and Environment, University of
9 Leeds, Leeds LS2 9JT, UK

10 Corresponding author: **Qiliang Sun** (sunqiliang@cug.edu.cn)

11

12 **Abstract**

13 Structures that facilitate fluid migration are common in sedimentary basins. We document several
14 possible hydrothermal and/or volcanic vents located above a $>157 \text{ km}^2$, late Cretaceous volcanic
15 field in the Great South Basin, offshore New Zealand. Three of the four vents are vertically
16 stacked, suggesting episodic re-use of the same fluid pathway between ~ 75 and ~ 56 Ma. A paleo-
17 pockmark dated to ~ 49 Ma and free gas occurring within strata ~ 21 Myr old are located directly
18 above these stacked vents. The spatial association of the vents, pockmark, and free gas further
19 suggests re-use of the fluid migration pathway(s) extended for over 54 Myr. Our results imply that
20 reutilization of fluid flow pathways can affect the distribution of fluids within basins over
21 prolonged periods, potentially impacting hydrocarbon/geothermal exploration and geohazard
22 assessment.

23 **Keywords**

24 Hydrothermal vent, fluid migration, gas chimney, pockmark, Great South Basin

25 **1 Introduction**

26 Focused fluid flow and associated fluid escape structures (e.g. hydrothermal vents, gas
27 chimneys, mud diapirs, and pockmarks) commonly occur in sedimentary basins (e.g. Bischoff et
28 al., 2019; Cartwright et al., 2007; Cartwright & Santamarina, 2015; Jackson et al., 2019; Jamtveit
29 et al., 2004; Siregar et al., 2019; Svensen et al., 2004). Many sedimentary basins also host a variety
30 of magmatic complexes (e.g. Jackson et al., 2013; Magee et al., 2014; Schofield et al., 2017; Song
31 et al., 2017). In addition to feeding and creating volcanoes, this magmatism can also produce
32 pockmarks and/or hydrothermal vents driven by magmatic volatile escape and intrusion-induced
33 heating of pore fluids (e.g. Iyer et al., 2017; Mourgues et al., 2012; Svensen et al., 2006). Although
34 these intrusion-related fluid escape structures form near-instantaneously (Planke et al., 2005),
35 identification of vertically stacked hydrothermal vent systems suggests intrusions can direct fluid
36 flow over millions of years (typically <10 Myr) (e.g. Roelofse et al., 2021). Similarly, the presence
37 of fluid and gas indicators above some hydrothermal vents and volcanic edifices implies that their
38 plumbing systems may be reactivated by and focus later fluid flow (e.g. hydrocarbon or carbon
39 dioxide) long after magmatism has ceased (e.g. Holford et al., 2017; Manton et al., 2022; Roelofse
40 et al., 2021; Sun et al., 2020a). Understanding the timeframes over which fluid escape structures
41 can be re-used may help improve the exploration efficiency of associated fluid-related resources
42 and aid de-risking of subsurface storage sites.

43 Here, we use 3D seismic reflection data from the Great South Basin, offshore New Zealand, to
44 image and date a large central volcanic edifice, overlying volcanic and/or hydrothermal vents, and

45 other fluid escape structures. The main volcanic edifice formed in the Late Cretaceous, above
46 which three, vertically stacked volcanic and/or hydrothermal vents formed between ~75 Ma and
47 ~56 Ma, seemingly sharing the same fluid migration pathway. In strata above these stacked vents
48 are: (1) an erosional depression (a pockmark), which probably formed due to surficial fluid escape
49 at ~49 Ma; and (2) a series of high-amplitude, negative-polarity reflections in shallower strata (~21
50 Myr old) that we suggest represent younger gas accumulations. Our analysis suggests that fluid
51 escape structures and migration pathways were reutilized on multiple occasions over a prolonged
52 time (~54 Myr), thereby influencing the distribution of fluids.

53 **2 Geological Setting**

54 Our study area is located within the Great South Basin (GSB), which is a rift basin located
55 offshore the southern tip of the South Island of New Zealand (Fig. 1). The GSB covers an area of
56 ~100,000 km² with present water depths of ~300 m to ~1000 m, and a maximum sedimentary
57 sequence thickness of ~8.5 km (Evans, 1982; Killops et al., 1997). This rift basin formed during
58 the Cretaceous breakup of Gondwana and comprises a series of graben and half-graben (Figs. 1a)
59 (Cook et al., 1999).

60 The syn-rift Hoiho Group (Late Cretaceous) deposited along the axis of graben is mainly
61 composed of terrestrial conglomerates, sandstones, shales, and coals (e.g., Killops et al., 1998;
62 Mitchell et al., 2009) (Fig. 2). The Hoiho Group has been penetrated by several wells (e.g. the
63 Tara-1 and Hoiho-1C) and is considered to be the principal hydrocarbon source rock in the GSB
64 (Beggs et al., 1990). Post-rift strata marking a transition from a continental to marine environment
65 were deposited between Late Cretaceous and Late Eocene, and can be sub-divided into the Pakaha
66 Group (Late Cretaceous - Late Paleocene) and the Rakiura Group (Eocene) (Figs. 2-3) (Cook et
67 al., 1999). The Pakaha Group is composed of the Kawau Formation (Late Cretaceous), Wickliffe
68 Formation (Late Cretaceous - Late Paleocene), Taratu Formation (Late Cretaceous), and Tartan
69 Formation (Late Paleocene - Paleocene) (Fig. 2). The Kawau Formation is mainly composed of
70 transgressive sandstones and directly overlies the Hoiho Group and basement (Osli et al., 2018;
71 Sahoo et al., 2022; Schiøler et al., 2010); the Kawau Formation is widely developed across the
72 GSB and serves as the main reservoir and lateral migration pathway for fluids (Killops et al., 1997)
73 (Fig. 2). The Wickliffe Formation is mainly composed of shale and clays (Chenrai, 2016;
74 Meadows, 2009), whereas the Taratu Formation is mainly composed of organic-rich clays and thus
75 forms one of the oil-prone formations in the basin (Osli et al., 2018; Shalaby et al., 2019). The
76 Rakiura Group can be divided into the Laing Formation (clays) (Eocene) and the Tucker Cove
77 Formation (marls) (Eocene) (Morley et al., 2017; Viskovic, 2010) (Fig. 2).

78 Intraplate igneous activity has occurred periodically across New Zealand, both onshore and
79 offshore (e.g. Barrier et al., 2021; Field et al., 1989; Hoernle et al., 2006, 2020; Omosanya et al.,
80 2021; Timm et al., 2009). Previous studies have divided the igneous activity across New Zealand
81 into four stages that corresponded to different tectonic periods (e.g., Barrier et al., 2021; Bischoff
82 et al., 2020). For example, syn-rift volcanism (105-83 Ma) associated with lithospheric thinning
83 and rifting caused by the break-up of Gondwana is observed across the Canterbury Basin (e.g. the
84 XXX) (Bischoff et al., 2020; Field et al., 1989; van der Meer et al., 2017). After rifting, the South
85 Island of New Zealand entered a period of intense magmatic activity (83-66 Ma), caused by the
86 separation of Zealandia from Australia and Antarctica (Barrier et al., 2021; Bischoff et al., 2020).
87 Large volcanoes and volcanic fields formed during this period, such as the main edifice of Tuatara
88 Volcanic Field (TVF) and associated sills and vents in the GSB (Phillips & Magee, 2020) and the
89 Galleon Volcanics (GV) in the offshore Canterbury Basin (Fig. 1a) (Tulloch et al., 2009). Igneous
90 activity at the Tuatara Volcanic Field continued periodically into the Early Eocene (to ~45 Ma),
91 during post-rift tectonic quiescence (Omosanya et al., 2021; Phillips & Magee, 2020). Other
92 monogenetic volcanic fields formed in the southwestern Pacific Plate (e.g. the Waiareka-Deborah
93 in New Zealand) during the Cenozoic (60-30 Ma), which was defined as diffuse intraplate
94 volcanism (Bischoff et al., 2020; Finn et al., 2005; Németh & Kereszturi, 2015; Scott et al., 2020).
95 The Papatowai Volcanic Field (PVF) in the GSB was formed during this period and covered an
96 area of >1600 km² (Bischoff et al., 2020) (Fig. 1). After the Miocene, intense magmatic activity
97 occurred onshore and offshore New Zealand associated with the Hikurangi subduction zone and
98 dextral strike-slip transgression along the Alpine Fault (Barrier et al., 2021; Bischoff et al., 2020;
99 Omosanya et al., 2021; Nicol et al., 2007).

100 **3 Data and Method**

101 We use high-resolution, time-migrated 3D seismic reflection data (the Twahaki-Rigel 3D) from
102 offshore the southern tip of the South Island of New Zealand (Fig. 1). The seismic survey covers
103 an area of ~4880 km² and was acquired between late 2011 and early 2012, using eight 6 km long
104 streamers. The data has a bin spacing of 6.25 × 37.5 m, a record length of 9.2 s, and a sampling
105 interval of 2 ms (resampled to 4 ms in the final processed data). The seismic data is zero-phase
106 processed and is displayed with the Society of Exploration Geophysicists (SEG) standard polarity,
107 whereby a downward increase in acoustic impedance (a function of rock velocity and density)
108 corresponds to a positive reflection event (red on seismic profiles) (Brown, 2011). Bertoni et al.
109 (2019) report that the vertical resolution of the seismic data is ~10 m in the shallow subseafloor
110 between ~1-2 s TWT, and is ~15-20 m between 2-3 s TWT.

111 We mapped nine regional stratigraphic boundaries/horizons: H2 (~21 Ma), T70 (~35 Ma), T60
112 (~42 Ma), T50 (~49 Ma), T10 (~56 Ma), H1 (~60 Ma), K100 (~66 Ma), K80 (~75 Ma), and K50

113 (~83 Ma) (Figs. 2-3). Horizon K50 represents the end of rifting, with horizons K100, T10, and
114 T70 marking the tops of the Cretaceous, Paleocene, and Eocene successions, respectively. Mapped
115 horizons, except for H1 and H2, were assigned an age based on previously reported
116 biostratigraphic data from 14 offshore wells (Bertoni et al., 2018, 2019; Blanke, 2015; Hunt
117 International Petroleum Co. NZ, 1977a, 1977b, 1977c, 1978a, 1978b, 1978c; Placid Oil Company,
118 1984a, 1984b; Sahoo et al., 2020, 2022; Schiøler & Raine, 2009; Schiøler et al., 2011, 2012, 2017)
119 (Fig. 2). The ages of Horizon H1 and H2 were estimated from the strata thickness to the upper and
120 lower adjacent horizons (e.g., T10, K100 and T70), with the assumption that the sedimentation
121 rates were consistent.

122 To help characterize possible fluid escape structures (e.g. mounded structures), we extracted
123 envelope and root mean square (RMS) attributes and variance slices from the 3D seismic volume.
124 The envelope is the total instantaneous energy of the analytic signal (the complex trace), which is
125 proportional to the reflection coefficient, and it is useful to identify discontinuities, lithologic
126 variations, and faults (Alves et al., 2015; Subrahmanyam and Rao, 2008). The RMS is a seismic
127 attribute that is commonly used to identify amplitude anomalies, whereas variance characterizes
128 differences in adjacent traces so highlights amplitude anomalies and discontinuities (e.g. faults,
129 igneous bodies, and channels) (Brown, 2011; Marfurt & Alves, 2014).

130 **4 Results**

131 4.1 Seismic characteristics of mounded structures

132 We observe a central edifice that comprises a series of stacked (up to 660 ms TWT thick),
133 discontinuous, often strata-concordant, low-to-high amplitude reflections developed at K50 (Fig.
134 3). Beneath this central edifice, seismic reflections are poorly imaged and appear blanked, likely
135 because overlying higher amplitude reflections have absorbed and/or scattered the seismic energy
136 (Fig. 3); the basal surface of the central edifice thus cannot be confidently identified. The central
137 edifice has a diameter of ~20 km and covers ~157 km² in the study area, although only part of the
138 central edifice is imaged by our seismic data (Fig. 3). The top of the central edifice is marked by
139 positive-polarity reflections and is onlapped by strata between horizons K50 and K80 (Fig. 3).
140 Within the central edifice, conical-like structures are apparent that internally comprise have weak-
141 to-chaotic seismic reflections (Fig. 3).

142 Four mounded structures are observed above the central edifice, within a vertical zone of chaotic
143 and dim seismic imaging, and we name them M1 to M4 from the oldest to the youngest (Figs. 4-
144 5, S1-S4). M1 appears to sit on top of the central edifice and Horizon K80 (~75 Ma), and has a
145 diameter of ~1.6 km and area of ~2.01 km² (Figs. 3, 4, and 5a). It has a height of ~810 ms TWT.
146 M2 is located ~2 km to the west of M1 (Figs. 3-4), and directly sits on top of Horizon K100 (~66

147 Ma; Fig. 5b). Among the four mounded structures, M2 has the largest diameter of ~ 3.8 km and
148 covers an area of ~ 11.34 km². M2 has a maximum height of ~ 900 ms TWT. M3 is located directly
149 on Horizon H1 (~ 60 Ma), and has a diameter of ~ 2.0 km, and an area of ~ 3.14 km² (Fig. 5c). M3
150 is ~ 250 ms TWT high. M4 sits on Horizon T10 (~ 56 Ma), 90 ms TWT above the summit of M1,
151 and is the smallest and youngest mounded structure; it covers an area of ~ 1.77 km², and has a
152 height of 140 ms TWT (Fig. 5d). M1, M3, and M4 are vertically stacked and although they occur
153 within a vertical seismically chaotic zone (see details in the next section), they can be confidently
154 identified from their conical shapes, sub-horizontal bases, and onlapping seismic reflections (Figs.
155 5-6, S1-S4). The tops of the mounded structures are usually characterized by weak, continuous,
156 positive-polarity seismic reflections (M1, M3, and M4; Figs. 5a, 5c-5d). However, a strong,
157 continuous, negative top is observed at M2 (Fig. 5b). The bases of mounded structures are flat or
158 rugose, with positive-polarity seismic reflections. Interiors of mounded structures are
159 characterized by chaotic seismic reflections (Fig. 5).

160 4.2 Depression and amplitude anomalies

161 A vertical chaotic zone, a sub-circular depression, and several high amplitude anomalies are
162 observed in the study area above the mounded structures (Figs. 3, 4, and 6-7). The vertical chaotic
163 zone is ~ 1.5 km wide and extends downward to Horizon T70, across the mounded structures, and
164 to the central edifice (Fig. 6). A sub-circular depression with a diameter of 2.5 km and a depth of
165 200 ms TWT occurs at T50. This depression is situated ~ 300 ms TWT above M4 and it truncates
166 underlying reflections (Figs. 6a-6c and 7). Strata within the depression onlap onto its side, and are
167 characterized by high-amplitude seismic reflections (Figs. 6a-6b). Stacked high-amplitude,
168 negative-polarity seismic anomalies occur at and around the top of the vertical chaotic zone
169 between horizons T50 and T70 (Figs. 7-8). Some isolated high amplitude anomalies with diameters
170 of 0.6-1.0 km also occur above Horizon T70 and can reach up to Horizon H2 (~ 21 Ma; Fig. 8).
171 These amplitude anomalies are sub-circular in plan-view and, on average, have areas of ~ 0.4 km².

172 5 Discussion

173 5.1 Mounded structure origins

174 The stacked, discontinuous, positive polarity, often strata-concordant, low-to-high amplitude
175 internal seismic reflections of the up to 660 ms TWT thick, >157 km² central edifice are similar to
176 those of nearby volcanic complexes, such as the Tuatara Volcanic Field (Phillips & Magee, 2020)
177 and the Papatowai Volcanic Field (Bischoff et al., 2020). Therefore, we interpret the central edifice
178 as a volcanic field; the conical structures within the edifice are likely volcanic vents and the strata-
179 concordant, high-amplitude reflections are probably eruptive products like lava flows (Fig. 3).

180 Based on seismic-stratigraphic onlap relationships, this volcanic field seemingly formed at K50
181 (83 Ma) and may have been active up to Horizon K80 (~75 Ma) (Fig. 3).

182 Seismic reflections onlapping onto the flanks of the mounded structures above the central edifice
183 indicate that they formed at the free surface and were subsequently buried by sediment (Figs. 6c
184 and 6f) (e.g. Hansen, 2006; Magee et al., 2021; Rateau et al., 2013; Smallwood & Maresh, 2002;
185 Trude et al., 2003). No boreholes have penetrated M1-M4, and thus their ages cannot be directly
186 dated. Yet by dating the age of onlapping and underlying reflections we can constrain the relative
187 ages of the mounded structures, and thus suggest M1-M4 formed at ~75 Ma, ~66 Ma, ~60 Ma,
188 and ~56 Ma, respectively (Fig. 5).

189 Mounded structures like M1-M4 are common in sedimentary basins and they have several
190 possible origins, including carbonate buildup, mud volcanism, igneous volcanism, and
191 hydrothermal venting (e.g., Burgess et al., 2013; Kirkham et al., 2018; Magee et al., 2013;
192 Reynolds et al., 2017; Schofield & Totterdell, 2008). Carbonate buildups usually reflect the
193 accumulation of organisms, such as reefs and algae, and in shallow-marine settings can have a
194 mounded appearance (Heckel, 1974). However, although deep-water carbonate buildups have
195 occasionally been reported, they do not form mounded structures with km-scale diameters and
196 hundred m-scale heights (e.g., Vlahović et al., 2005). Given our study area was situated in a deep-
197 water regime since ~75 Ma (Higgs et al., 2021; Killops et al., 1997; Osli et al., 2018; Shalaby et
198 al., 2019), and the scale of the mounded structures mapped, we consider it unlikely that the
199 mounded structures represent carbonate buildups.

200 Mud volcanoes usually occur above massive muddy deposits (Dimitrov, 2002; Mazzini &
201 Etiope, 2017). Based on our interpretation, M1 likely sits on a volcanic field comprising stacked
202 lavas and volcanoclastics, perhaps with some interbedded sedimentary strata (Phillips and Magee,
203 2020). The presence of predominantly igneous material beneath M1 and the thin stratal layers
204 between the volcanic field and other mounded structures (especially M1 and M2), would likely
205 limit the availability of mud, implying the mounded structures are probably not mud volcanoes
206 (Figs. 3 and 6).

207 Igneous volcanoes mainly comprise crystalline lavas or volcanoclastic rocks that are typically
208 denser and have higher seismic velocities than those of surrounding sedimentary rocks (e.g.,
209 Calvès et al., 2011). We thus expect buried igneous volcanoes to show high-amplitude, positive
210 seismic reflections at their tops (cf., Magee et al., 2013; Reynolds et al., 2018; Sun et al., 2019;
211 Zhao et al., 2016). Yet we observe moderate-to-weak seismic reflections across the tops of M1-
212 M4, as well as the negative top of M2 (Figs. 5b and 6d), which seem inconsistent with an igneous
213 volcano origin. However, we note that M1, M3, and M4 occur in a vertical chaotic zone where the
214 seismic reflection data is dimmer than elsewhere, which may have muted the amplitude response

215 of these mounded structures; i.e. we cannot rule out that they are volcanic vents. We also recognize
216 that the negative polarity top of M2 could reflect the presence of an altered hyaloclastite layer
217 blanketing the mound, whereby the alteration has reduced its density and seismic velocity to below
218 that of the overlying Paleocene strata (Ellefsen et al., 2010). Alternatively, our mounded structures
219 also appear similar to hydrothermal vents, which usually contain chaotic internal seismic
220 reflections, have conical/crater/eye-like shapes, and weak-moderate tops (usually positive
221 polarity), such as those documented in the offshore southern Australia (Jackson, 2012), the Møre
222 Basin (Kjoberg et al., 2017; Planke et al., 2005) and the Qiongdongnan Basin (Wang et al., 2019).
223 If M1, M3, and/or M4 are hydrothermal vents, their flat bases (Figs. 5b-5d) would suggest the
224 fluids were probably released slowly from the subsurface into the overlying water column, and
225 thus they did not eject shallow sediments to form a crater (Planke et al., 2005). Hydrothermal vents
226 are often related to underlying magma intrusions (cf., Jackson, 2012; Planke et al., 2005). Although
227 we observe no sills that directly connect to M1-M4, the presence of these vents above the volcanic
228 field may suggest that magmatism, or at least the generation and migration of hydrothermal fluids
229 within this area, occurred after the formation of main edifice in the volcanic field.

230 5.2 Reutilization of fluid escape structures

231 Because M1, M3, and M4 are vertically stacked and appear within the same vertical chaotic
232 zone (Figs. 4, 6, and 9a), it seems reasonable to suggest that the younger vents may have reutilized
233 the fluid feeder conduits of older vents; i.e. fluid flow was focused by pre-existing structures for
234 ~17 Myrs. Roelofse et al (2021) similarly showed two stacked hydrothermal vents in the Modgunn
235 Arch of the Norwegian Sea, formed at Late Cretaceous and Late Paleocenes, supporting our
236 interpretation that hydrothermal fluid pathways can remain open for prolonged periods.

237 We observe that the vertical chaotic zone continues above M4 and is associated with stacked
238 high-amplitude, negative polarity anomalies up to Horizon T70 (Fig. 6); together, these features
239 resemble the typical seismic characteristics of gas chimneys and free gas (Cartwright &
240 Santamarina, 2015; Gross et al., 2018; Løseth et al., 2011). In such systems, vertical chaotic zones
241 like we observe are caused by the absorption of acoustic energy in overlying high-amplitude strata,
242 which hinders the downward transmission of energy to the underlying fluid feeder system (Roy et
243 al., 2016). Considering the gas accumulates within strata as young as Horizon H2 (~21 Ma), at
244 least some gas-charging events were younger than ~21 Ma.

245 The depression observed within the gas chimney at Horizon T50 shows evidence of erosion as
246 it truncates underlying reflections and contains reflections that onlap onto its sides (Figs. 7a-7b);
247 these features suggest the depression formed at the contemporaneous seafloor at ~49 Ma, perhaps
248 in response to fluid escape (c.f., Cartwright, 2007). We specifically interpret the depression as a

249 pockmark because its bowl-like geometry, size, and seismic-stratigraphic relationship are similar
250 to pockmarks observed elsewhere (Ho et al., 2018; Velayatham et al., 2018).

251 Because there are no borehole samples available from the interpreted ~49-21 Myr old gas
252 chimney, pockmark, or free gas anomalies, we cannot ascertain the composition of the fluids
253 involved in their formation, but we consider three possible origins: 1) hydrothermal fluids (e.g.,
254 CO₂) related to magmatic activity, perhaps similar to those that may have generated M1-M4 if
255 they are hydrothermal vents (Niyazi et al., 2021; Sharma & Srivastava, 2014); 2) hydrocarbons
256 generated from source rocks of the Hoiho Group (Killops et al., 1997; Omosanya & Harishidayat,
257 2019; Shalaby et al., 2019); or 3) a mixture of the above-mentioned two sources. With regards to
258 hydrothermal activity, we note that there was a regional reduction in magmatic activity during
259 tectonic quiescence between 66 Ma and 30 Ma (Bischoff et al., 2020). Such waning hydrothermal
260 and magmatic activity may suggest the gas chimney and free gas anomalies, as well as the
261 pockmark, did not form in response to hydrothermal fluid escape. Instead, it seems plausible that
262 the fluid escape structures and free gas were produced by the release of hydrocarbons. We suggest
263 that the porous sandstone of the Kawau Formation, which surrounded the volcanic field in the
264 study area, and/or the fluid plumbing system of the hydrothermal vents M1, M3, and M4 may have
265 provided a pathway for hydrocarbon migration from the deep-seated source rocks in the Hoiho
266 Group (Figs. 7b and 9b). The migrating hydrocarbons may have temporarily accumulated around
267 the peak of M4, because of its mounded morphology. When the overpressure exceeded the yield
268 strength of overlying strata, the gas chimney (hydraulic fracturing) would have developed above
269 M4. The explosive release of overpressured fluids through the gas chimney may have led to the
270 disaggregation and expulsion of unconsolidated, shallow seabed sediments to form the observed
271 pockmark (Figs. 7 and 9b). The widespread free gas anomalies, which extend upwards to Horizon
272 H2 suggest that the gas chimney was active, either continuously or episodically, until at least to
273 ~21 Ma (Horizon H2) (Fig. 9c).

274 Overall, our interpretation suggests that the M1, M3, and M4 vents and their plumbing system
275 were utilized for fluid flow over 54 Myrs. The longevity of fluid flow pathways probably played
276 important roles (providing hydrocarbon migration pathways) in linking the source rocks to the
277 overlying reservoirs when the source rocks were deeply buried (mature), such as those in the Faroe-
278 Shetland basins (Schofield et al., 2017) and the South China Sea (Sun et al., 2020a). Therefore,
279 the longevity of fluid flow pathways may promote the accumulation of fluids (e.g. hydrocarbon).
280 However, the longevity of fluid flow may also trigger seabed instability, when the transported
281 fluids accumulate within the shallow strata or erupt onto the seabed. In general, reassessment of
282 the hydrocarbon/geothermal exploration and geohazard assessment may be needed, where the
283 longevity and reutilization of fluid flow pathways occur.

284 **6 Conclusions**

285 We examine a series of vertically stacked and connected fluid escape structures using high-
286 resolution 3D seismic reflection data from the Great South Basin, offshore the South Island of
287 New Zealand. Specifically, we recognize four hydrothermal and/or volcanic vents located above
288 a huge ancient volcanic field formed in the Late Cretaceous. The hydrothermal and/or volcanic
289 vents formed periodically at ~75 Ma, ~66 Ma, ~60 Ma, and ~56 Ma, respectively. Fluid flow
290 features including a gas chimney, a pockmark, and gas-charged strata are observed above these
291 stacked vents and at least formed between ~49 Ma and ~21 Ma. The observed stacking of vents, a
292 pockmark, and gas accumulations suggests that the fluid escape pathway was probably re-used
293 multiple times over 54 Myr. This study indicates that reutilization of fluid flow pathways can
294 control the distribution of fluids within basins over prolonged periods.

295

296 **Acknowledgments**

297 The authors thank the New Zealand Petroleum and Minerals for making the seismic reflection
298 data used in this study publicly available. Deputy Editor Kerry Gallagher, and two reviewers, Dr.
299 Hehe Chen and Dr. Nick Schofield are thanked for their constructive comments and suggestions
300 that greatly improve this paper.

301 **Open Research**

302 3D seismic reflection data used in the study is available at the New Zealand Petroleum & Minerals Online
303 Exploration Database (<https://data.nzpam.govt.nz/GOLD/system/mainframe.asp>).

304 **References**

- 305 Alves, T. M., Omosanya, K. d., & Gowling, P. (2015). Volume rendering of enigmatic high-amplitude
306 anomalies in southeast Brazil: A workflow to distinguish lithologic features from fluid accumulations.
307 *Interpretation*, 3(2), 1-14. <http://doi.org/10.1190/INT-2014-0106.1>
- 308 Bache, F., Sutherland, R., Stagpoole, V., Herzer, R., Collot, J., & Rouillard, P. (2012). Stratigraphy of the
309 southern Norfolk Ridge and the Reinga Basin: A record of initiation of Tonga–Kermadec–Northland
310 subduction in the southwest Pacific. *Earth and Planetary Science Letters*, 321-322, 41-53.
311 <https://doi.org/10.1016/j.epsl.2011.12.041>
- 312 Bache, F., Mortimer, N., Sutherland, R., Collot, J., Rouillard, P., Stagpoole, V., & Nicol, A. (2014). Seismic
313 stratigraphic record of transition from Mesozoic subduction to continental breakup in the Zealandia sector of
314 eastern Gondwana. *Gondwana Research*, 26(3-4), 1060-1078. <https://doi.org/10.1016/j.gr.2013.08.012>
- 315 Barrier, A., Bischoff, A., Nicol, A., Browne, G. H., & Bassett, K. N. (2021). Relationships between volcanism
316 and plate tectonics: A case-study from the Canterbury Basin, New Zealand. *Marine Geology*, 433(433),

317 106397. <https://doi.org/10.1016/j.margeo.2020.106397>

318 Beggs, J. M., Challis, G. A., & Cook, R. A. (1990). Basement geology of the Campbell Plateau: Implications
319 for correlation of the Campbell Magnetic Anomaly System. *New Zealand Journal of Geology and Geophysics*,
320 33(3), 401-404. <https://doi.org/10.1080/00288306.1990.10425696>

321 Bertoni, C., Cartwright, J., Foschi, M., & Martin, J. (2018). Spectrum of gas migration phenomena across
322 multilayered sealing sequences. *AAPG Bulletin*, 102(6), 1011-1034.
323 <https://doi.org/10.1306/0810171622617210>

324 Bertoni, C., Gan, Y., Paganoni, M., Mayer, J., Cartwright, J., Martin, J., van Rensbergen, P., Wunderlich, A., &
325 Clare, A. (2019). Late Paleocene pipe swarm in the Great South – Canterbury Basin (New Zealand). *Marine*
326 *and Petroleum Geology*, 107, 451-466. <https://doi.org/10.1016/j.marpetgeo.2019.05.039>

327 Bischoff, A., Nicol, A., Barrier, A., & Wang, H. (2019). Paleogeography and volcanic morphology
328 reconstruction of a buried monogenetic volcanic field (part 2). *Bulletin of Volcanology*, 81(9), 57.
329 <https://doi.org/10.1007/s00445-019-1317-6>

330 Bischoff, A., Barrier, A., Beggs, M., Nicol, A., Cole, J., & Sahoo, T. (2020). Volcanoes buried in Te Riu-a-
331 Māui/Zealandia sedimentary basins. *New Zealand Journal of Geology and Geophysics*, 63(4), 378-401.
332 <https://doi.org/10.1080/00288306.2020.1773510>

333 [Blanke, S. \(2015\). PEP 38264 Caravel - 1 well completion report. In *New Zealand Petroleum Report*
334 *\(PR4896\)*.](#)

335 Brown, A. R. (2011). *Interpretation of three-dimensional seismic data*, 7th ed., Society of Exploration
336 Geophysicists and American Association of Petroleum Geologists, Tulsa, Okla.

337 Burgess, P. M., Winefield, P., Minzoni, M., & Elders, C. (2013). Methods for identification of isolated
338 carbonate buildups from seismic reflection data. *AAPG Bulletin*, 97(7), 1071-1098.
339 <https://doi.org/10.1306/12051212011>

340 Calvès, G., Schwab, A. M., Huuse, M., Clift, P. D., Gaina, C., Jolley, D., Tabrez, A. R., & Inam, A. (2011).
341 Seismic volcanostratigraphy of the western Indian rifted margin: The pre-Deccan igneous province. *Journal of*
342 *Geophysical Research: Solid Earth*, 116(B1). <https://doi.org/10.1029/2010JB000862>

343 Cartwright, J. (2007). The impact of 3D seismic data on the understanding of compaction, fluid flow and
344 diagenesis in sedimentary basins. *Journal of the Geological Society*, 164(5), 881. <http://doi.org/10.1144/0016-76492006-143>

346 Cartwright, J., & Santamarina, C. (2015). Seismic characteristics of fluid escape pipes in sedimentary basins:
347 Implications for pipe genesis. *Marine and Petroleum Geology*, 65, 126-140.
348 <https://doi.org/10.1016/j.marpetgeo.2015.03.023>

349 Chenrai, P. (2016). Seismic stratigraphy and fluid flow in the Taranaki and Great South Basins offshore New
350 Zealand. The University of Manchester (United Kingdom).

351 Cook, R. A., Sutherland, R., & Zhu, H. (1999). *Cretaceous-Cenozoic Geology and Petroleum Systems of the*
352 *Great South Basin, New Zealand*, Institute of Geological & Nuclear Sciences, Lower Hutt, New Zealand.

353 Dimitrov, L. I. (2002). Mud volcanoes—the most important pathway for degassing deeply buried sediments.
354 *Earth-Science Reviews*, 59(1), 49-76. [https://doi.org/10.1016/S0012-8252\(02\)00069-7](https://doi.org/10.1016/S0012-8252(02)00069-7)

355 Eichhubl, P., Davatz, N. C., & Becker, S. P. (2009). Structural and diagenetic control of fluid migration and
356 cementation along the Moab fault, Utah. *AAPG Bulletin*, 93(5), 653-681. <https://doi.org/10.1306/02180908080>

357 Ellefsen, M., Boldreel, L. O., & Larsen, M. (2010). Intra-basalt units and base of the volcanic succession east
358 of the Faroe Islands exemplified by interpretation of offshore 3D seismic data. *Geological Society, London,*
359 *Petroleum Geology Conference Series*, 7(1), 1033-1042. <https://doi.org/10.1144/0071033>

360 Evans, P. R. (1982). Petroleum potential of New Zealand. *Journal of Petroleum Geology*, 5(1), 89-96.
361 <https://doi.org/10.1111/j.1747-5457.1982.tb00562.x>

362 Field, B. D., Browne, G. H., Davy, B. W., & Survey, N. Z. G. (1989). *Cretaceous and Cenozoic Sedimentary*
363 *Basins and Geological Evolution of the Canterbury Region, South Island, New Zealand*, New Zealand
364 Geological Survey.

365 Gross, F., et al. (2018). Free gas distribution and basal shear zone development in a subaqueous landslide –
366 Insight from 3D seismic imaging of the Tuaheni Landslide Complex, New Zealand. *Earth and Planetary*
367 *Science Letters*, 502, 231-243. <https://doi.org/10.1016/j.epsl.2018.09.002>

368 Hansen, D. M. (2006). The morphology of intrusion-related vent structures and their implications for
369 constraining the timing of intrusive events along the NE Atlantic margin. *Journal of the Geological Society*,
370 *163*(5), 789. <https://doi.org/10.1144/0016-76492004-167>

371 Hart, B. S., & Hamilton, T. S. (1993). High-resolution acoustic mapping of shallow gas in unconsolidated
372 sediments beneath the strait of Georgia, British Columbia. *Geo-Marine Letters*, 13(1), 49-55.
373 <http://doi.org/10.1007/BF01204392>

374 Heckel, P. H. (1974). Carbonate Buildups in the Geologic Record: A Review, in *Reefs in Time and Space:*
375 *Selected Examples from the Recent and Ancient*, edited by Laporte, L. F., p. 0, SEPM Society for Sedimentary
376 Geology, <http://doi.org/10.2110/pec.74.18.0090>

377 Higgs, K. E., Funnell, R. H., & Browne, G. H. (2021). A multidisciplinary study of diagenesis and pore fluid
378 evolution in frontier basins; an example from Canterbury and Great South basins, New Zealand. *Marine and*
379 *Petroleum Geology*, 124, 104817. <https://doi.org/10.1016/j.marpetgeo.2020.104817>

380 Ho, S., Imbert, P., Hovland, M., Wetzel, A., Blouet, J.-P., & Carruthers, D. (2018). Downslope-shifting
381 pockmarks: interplay between hydrocarbon leakage, sedimentations, currents and slope's topography.
382 *International Journal of Earth Sciences*, 107(8), 2907-2929. <https://doi.org/10.1007/s00531-018-1635-5>

383 Hoernle, K., White, J. D. L., van den Bogaard, P., Hauff, F., Coombs, D. S., Werner, R., Timm, C., Garbe-
384 Schönberg, D., Reay, A., & Cooper, A. F. (2006). Cenozoic intraplate volcanism on New Zealand: Upwelling
385 induced by lithospheric removal. *Earth and Planetary Science Letters*, 248(1-2), 350-367.
386 <https://doi.org/10.1016/j.epsl.2006.06.001>

387 Hoernle, K., Timm, C., Hauff, F., Tappenden, V., Werner, R., Jolis, E. M., Mortimer, N., Weaver, S., Riefstahl,
388 F., & Gohl, K. (2020). Late Cretaceous (99-69 Ma) basaltic intraplate volcanism on and around Zealandia:

389 Tracing upper mantle geodynamics from Hikurangi Plateau collision to Gondwana breakup and beyond. *Earth*
390 *and Planetary Science Letters*, 529, 115864. <https://doi.org/10.1016/j.epsl.2019.115864>

391 Holford, S. P., Schofield, N., & Reynolds, P. (2017). Subsurface fluid flow focused by buried volcanoes in
392 sedimentary basins: Evidence from 3D seismic data, Bass Basin, offshore southeastern Australia.
393 *Interpretation*, 5(3), SK39-SK50. <https://doi.org/10.1190/INT-2016-0205.1>

394 Hunt International Petroleum Co NZ. (1977a). Toroa-1 well completion report. In *New Zealand Petroleum*
395 *Report*, PR691.

396 Hunt International Petroleum Co NZ. (1977b). Final report Kawau-1A. In *New Zealand Petroleum Report*,
397 PR716.

398 Hunt International Petroleum Co NZ. (1977c). Pakaha-1 well completion report. In *New Zealand Petroleum*
399 *Report*, PR703.

400 Hunt International Petroleum Co NZ. (1978a). Hoiho-1C well completion report. In *New Zealand Petroleum*
401 *Report*, PR730.

402 Hunt International Petroleum Co NZ. (1978b). Tara-1 well completion report. In *New Zealand Petroleum*
403 *Report*, PR732.

404 Hunt International Petroleum Co NZ. (1978c). Takapu-1 & Takapu-1A well completion report. In *New*
405 *Zealand Petroleum Report*, PR733.

406 Iyer, K., Schmid, D. W., Planke, S., & Millett, J. (2017). Modelling hydrothermal venting in volcanic
407 sedimentary basins: Impact on hydrocarbon maturation and paleoclimate. *Earth and Planetary Science Letters*,
408 467, 30-42. <http://doi.org/10.1016/j.epsl.2017.03.023>

409 [Jackson, C. A. L., Schofield, N., & Golenkov. \(2013\). Geometry and controls on the development of igneous](https://doi.org/10.1130/B30833.1)
410 [sill-related forced folds: A 2-D seismic reflection case study from offshore southern Australia. *GSA Bulletin*,](https://doi.org/10.1130/B30833.1)
411 [125\(11-12\), 1874-1890. https://doi.org/10.1130/B30833.1](https://doi.org/10.1130/B30833.1)

412 Jackson, C. A. L. (2012). Seismic reflection imaging and controls on the preservation of ancient sill-fed
413 magmatic vents. *Journal of the Geological Society*, 169(5), 503-506. [https://doi.org/10.1144/0016-76492011-](https://doi.org/10.1144/0016-76492011-147)
414 [147](https://doi.org/10.1144/0016-76492011-147)

415 Jackson, C. A. L., Magee, C., & Hunt-Stewart, E. R. (2019). Cenozoic Contourites in the Eastern Great
416 Australian Bight, Offshore Southern Australia: Implications For the Onset of the Leeuwin Current. *Journal of*
417 *Sedimentary Research*, 89(3), 199-206. <https://doi.org/10.2110/jsr.2019.16>

418 Jamtveit, B., Svensen, H., Podladchikov, Y. Y., & Planke, S. (2004). Hydrothermal vent complexes associated
419 with sill intrusions in sedimentary basins. *Geological Society, London, Special Publications*, 234(1), 233.
420 <https://doi.org/10.1144/GSL.SP.2004.234.01.15>

421 Killops, S. D., Cook, R. A., Sykes, R., & Boudou, J. P. (1997). Petroleum potential and oil - source correlation
422 in the Great South and Canterbury Basins. *New Zealand Journal of Geology and Geophysics*, 40(4), 405-423.
423 <https://doi.org/10.1080/00288306.1997.9514773>

424 Killops, S. D., Funnell, R. H., Suggate, R. P., Sykes, R., Peters, K. E., Walters, C., Woolhouse, A. D., Weston,

425 R. J., & Boudou, J. P. (1998). Predicting generation and expulsion of paraffinic oil from vitrinite-rich coals.
426 *Organic Geochemistry*, 29(1), 1-21. [https://doi.org/10.1016/S0146-6380\(98\)00087-4](https://doi.org/10.1016/S0146-6380(98)00087-4)

427 Kirkham, C., Cartwright, J., Hermanrud, C., & Jebsen, C. (2018). The genesis of mud volcano conduits
428 through thick evaporite sequences. *Basin Research*, 30(2), 217-236. <https://doi.org/10.1111/bre.12250>

429 Kjoberg, S., et al. (2017). 3D structure and formation of hydrothermal vent complexes at the Paleocene-Eocene
430 transition, the Møre Basin, mid-Norwegian margin. *Interpretation*, 5(3), SK65-SK81.
431 <https://doi.org/10.1190/INT-2016-0159.1>

432 Løseth, H., Wensaas, L., Arntsen, B., Hanken, N.-M., Basire, C., & Graue, K. (2011). 1000 m long gas blow-
433 out pipes. *Marine and Petroleum Geology*, 28(5), 1047-1060. <https://doi.org/10.1016/j.marpetgeo.2010.10.001>

434 Magee, C., Hunt-Stewart, E., & Jackson, C. A. L. (2013). Volcano growth mechanisms and the role of sub-
435 volcanic intrusions: Insights from 2D seismic reflection data. *Earth and Planetary Science Letters*, 373, 41-53.
436 <https://doi.org/10.1016/j.epsl.2013.04.041>

437 [Magee, C., Jackson, C. A. L., & Schofield, N. \(2014\). Diachronous sub-volcanic intrusion along deep-water](https://doi.org/10.1111/bre.12044)
438 [margins: insights from the Irish Rockall Basin. *Basin Research*, 26\(1\), 85-105.](https://doi.org/10.1111/bre.12044)
439 <https://doi.org/10.1111/bre.12044>

440 Magee, C., Pichel, L. M., Madden - Nadeau, A. L., Jackson, C. A. L., & Mohriak, W. (2021). Salt–magma
441 interactions influence intrusion distribution and salt tectonics in the Santos Basin, offshore Brazil. *Basin*
442 *Research*, 33(3), 1820-1843. <https://doi.org/10.1111/bre.12537>

443 Manton, B., Müller, P., Mazzini, A., Zastrozhnov, D., Jerram, D.A., Millett, J.M., Schmid, D.W., Berndt, C.,
444 Myklebust, R., Planke, S., 2022. Characterizing ancient and modern hydrothermal venting systems. *Marine*
445 *Geology*, 447, 106781. <https://doi.org/10.1016/j.marpetgeo.2022.106781>

446 Marfurt, K. J., & Alves, T. M. (2014). Pitfalls and limitations in seismic attribute interpretation of tectonic
447 features. *Interpretation*, 3(1), SB5-SB15. <https://doi.org/10.1190/INT-2014-0122.1>

448 Mazzini, A., & Etiope, G. (2017). Mud volcanism: An updated review. *Earth-Science Reviews*, 168, 81-112.
449 <https://doi.org/10.1016/j.earscirev.2017.03.001>

450 Meadows, D. J. (2009). Stable isotope geochemistry of Paleocene to Early Eocene strata around southern New
451 Zealand. Victoria University of Wellington.

452 Mitchell, M., Craw, D., Landis, C. A., & Frew, R. (2009). Stratigraphy, provenance, and diagenesis of the
453 Cretaceous Horse Range Formation, east Otago, New Zealand. *New Zealand Journal of Geology and*
454 *Geophysics*, 52(3), 171-183. <https://doi.org/10.1080/00288300909509884>

455 Morley, C. K., Maczak, A., Rungprom, T., Ghosh, J., Cartwright, J. A., Bertoni, C., & Panpichityota, N.
456 (2017). New style of honeycomb structures revealed on 3D seismic data indicate widespread diagenesis
457 offshore Great South Basin, New Zealand. *Marine and Petroleum Geology*, 86, 140-154.
458 <https://doi.org/10.1016/j.marpetgeo.2017.05.035>

459 Mourgues, R., Bureau, D., Bodet, L., Gay, A., & Gressier, J. B. (2012). Formation of conical fractures in
460 sedimentary basins: Experiments involving pore fluids and implications for sandstone intrusion mechanisms.

461 *Earth and Planetary Science Letters*, 313-314, 67-78. <https://doi.org/10.1016/j.epsl.2011.10.029>

462 Nader, F. H., Swennen, R., & Ellam, R. (2004). Reflux stratabound dolostone and hydrothermal volcanism-
463 associated dolostone: a two-stage dolomitization model (Jurassic, Lebanon). *Sedimentology*, 51(2), 339-360.
464 <https://doi.org/10.1111/j.1365-3091.2004.00629.x>

465 Németh, K., & Kereszturi, G. (2015). Monogenetic volcanism: personal views and discussion. *International*
466 *Journal of Earth Sciences*, 104(8), 2131-2146. <https://doi.org/10.1007/s00531-015-1243-6>

467 Nicol, A., Mazengarb, C., Chanier, F., Rait, G., Uruski, C., & Wallace, L. (2007). Tectonic evolution of the
468 active Hikurangi subduction margin, New Zealand, since the Oligocene. *Tectonics*, 26(4).
469 <https://doi.org/10.1029/2006TC002090>

470 Niyazi, Y., Warne, M., & Ierodiaconou, D. (2021). Post-rift magmatism and hydrothermal activity in the
471 central offshore Otway Basin and implications for igneous plumbing systems. *Marine Geology*, 438, 106538.
472 <https://doi.org/10.1016/j.margeo.2021.106538>

473 Omosanya, K. O., & Harishidayat, D. (2019). Seismic geomorphology of Cenozoic slope deposits and deltaic
474 clinoforms in the Great South Basin (GSB) offshore New Zealand. *Geo-Marine Letters*, 39(1), 77-99.
475 <http://doi.org/10.1007/s00367-018-00558-8>

476 Omosanya, K. O., Lawal, M. A., Iqbal, H. M., & Yizhaq, M. (2021). Massive seafloor mounds depict potential
477 for seafloor mineral deposits in the Great South Basin (GSB) offshore New Zealand. *Scientific Reports*, 11(1),
478 9185. <https://doi.org/10.1038/s41598-021-88620-x>

479 Osli, L. N., Shalaby, M. R., & Islam, M. A. (2018). Hydrocarbon generation modeling and source rock
480 characterization of the Cretaceous–Paleocene Taratu Formation, Great South Basin, New Zealand. *Journal of*
481 *Petroleum Exploration and Production Technology*, 9(1), 125-139. <https://doi.org/10.1007/s13202-018-0511-y>

482 Phillips, T. B., & McCaffrey, K. J. W. (2019). Terrane Boundary Reactivation, Barriers to Lateral Fault
483 Propagation and Reactivated Fabrics: Rifting Across the Median Batholith Zone, Great South Basin, New
484 Zealand. *Tectonics*, 38(11), 4027-4053. <https://doi.org/10.1029/2019TC005772>

485 Phillips, T. B., & Magee, C. (2020). Structural controls on the location, geometry and longevity of an intraplate
486 volcanic system: the Tuatara Volcanic Field, Great South Basin, New Zealand. *Journal of the Geological*
487 *Society*, 177(5), 1039-1056. <https://doi.org/10.1144/jgs2020-050>

488 Placid Oil Company. (1984a). Well report, Rakiura - 1, Great South Basin, New Zealand. In *New Zealand*
489 *Petroleum Report*, PR994.

490 Placid Oil Company. (1984b). Final geological well completion report, Pukaki - 1, Great South Basin, New
491 Zealand, PPL38081. In *New Zealand Petroleum Report*, PR1005.

492 Planke, S., Rasmussen, T., Rey, S. S., & Myklebust, R. (2005). Seismic characteristics and distribution of
493 volcanic intrusions and hydrothermal vent complexes in the Vøring and Møre basins. *Geological Society,*
494 *London, Petroleum Geology Conference*, 6(1), 833. <https://doi.org/10.1144/0060833>

495 Rateau, R., Schofield, N., & Smith, M. (2013). The potential role of igneous intrusions on hydrocarbon
496 migration, West of Shetland. *Petroleum Geoscience*, 19(3), 259-272. <https://doi.org/10.1144/petgeo2012-035>

497 Reynolds, P., Holford, S., Schofield, N., & Ross, A. (2017). The shallow depth emplacement of mafic
498 intrusions on a magma-poor rifted margin: An example from the Bight Basin, southern Australia. *Marine and*
499 *Petroleum Geology*, 88, 605-616. <http://doi.org/10.1016/j.marpetgeo.2017.09.008>

500 Reynolds, P., Schofield, N., Brown, R. J., & Holford, S. P. (2018). The architecture of submarine monogenetic
501 volcanoes - insights from 3D seismic data. *Basin Research*, 30, 437-451. <https://doi.org/10.1111/bre.12230>

502 Roelofse, C., Alves, T. M., & Omosanya, K. d. O. (2021). Reutilisation of hydrothermal vent complexes for
503 focused fluid flow on continental margins (Modgunn Arch, Norwegian Sea). *Basin Research*, 33(2), 1111-
504 1134. <https://doi.org/10.1111/bre.12507>

505 Roy, S., Hovland, M., & Braathen, A. (2016). Evidence of fluid seepage in Grønfjorden, Spitsbergen:
506 Implications from an integrated acoustic study of seafloor morphology, marine sediments and tectonics.
507 *Marine Geology*, 380, 67-78. <https://doi.org/10.1016/j.margeo.2016.07.002>

508 Sahoo, T. R., Strogon, D. P., Browne, G. H., & Nicol, A. (2022). Evolution of syn- to early post-rift facies in
509 rift basins: insights from the Cretaceous–Paleocene of the Great South Basin, New Zealand. *Basin Research*,
510 34(3), 1113-1142. <https://doi.org/10.1111/bre.12652>

511 Schofield, A., Holford, S., Millett, J., Brown, D., Jolley, D., Passey, S. R., Muirhead, D., Grove, C., Magee, C.,
512 Murray, J., Hole, M., Jackson, C. A. -L., & Stevenson, C., 2017. Regional magma plumbing and emplacement
513 mechanisms of the Faroe-Shetland Sill Complex: implications for magma transport and petroleum systems
514 within sedimentary basins. *Basin Research*, 29, 41-63. <https://doi.org/10.1111/bre.12164>.

515 Schofield, A., Totterdell, J., 2008. *Distribution, Timing and Origin of Magmatism in the Bight and Eucla*
516 *Basins*, p. 19. Geoscience Australia Record 2008/24.

517 Schiøler, P., Rogers, K., Sykes, R., Hollis, C. J., Ilg, B., Meadows, D., Roncaglia, L., & Uruski, C. (2010).
518 Palynofacies, organic geochemistry and depositional environment of the Tartan Formation (Late Paleocene), a
519 potential source rock in the Great South Basin, New Zealand. *Marine and Petroleum Geology*, 27(2), 351-369.
520 <https://doi.org/10.1016/j.marpetgeo.2009.09.006>

521 Schiøler, P., & Raine, J. I. (2009). Palynology of lower Hoiho Group in the Great South Basin and Clipper and
522 Horse Range Formations in the Canterbury Basin, GNS Science Consultancy Report, 2009/361. In *New*
523 *Zealand Petroleum Report* (PR4348, pp. 1–67).

524 Schiøler, P., Raine, J. I., Crundwell, M. P., Griffin, A., Hollis, C. J., Kulhanek, D. K., et al. (2011). Revised
525 biostratigraphy and well correlation, Canterbury Basin, New Zealand, GNS Science Consultancy Report
526 2011/12. In *New Zealand Petroleum Report* (PR4365, pp. 1–142).

527 Schiøler, P., Raine, J. I., Crundwell, M. P., Fohrmann, M., Griffin, A., Hollis, C. J., et al. (2012). Revised
528 biostratigraphy and well correlation, Canterbury Basin, New Zealand; updated with results from Cutter-1 well.
529 GNS Science Consultancy Report, 2012/248, 164 p. in *New Zealand Petroleum Report*, PR4621.

530 Schiøler, P., Browne, G. H., Cameron, H., King, P. R., Strogon, D. P., Sahoo, T., & Funnell, R. H. (2017).
531 Great South Basin: National wells audit pilot project play analysis report, GNS Science Consultancy Report
532 2017/20. In *New Zealand Petroleum Report* (PR5428, pp. 1–70).

533 Scott, J. M., Pontesilli, A., Brenna, M., White, J. D. L., Giacalone, E., Palin, J. M., & le Roux, P. J. (2020). The
534 Dunedin Volcanic Group and a revised model for Zealandia's alkaline intraplate volcanism. *New Zealand*
535 *Journal of Geology and Geophysics*, 63(4), <http://doi.org/510-529.10.1080/00288306.2019.1707695>

536 Shalaby, M. R., Oslı, L. N., Kalaitzidis, S., & Islam, M. A. (2019). Thermal maturity and depositional
537 palaeoenvironments of the Cretaceous-Palaeocene source rock Taratu Formation, Great South Basin, New
538 Zealand. *Journal of Petroleum Science and Engineering*, 181, 106156.
539 <https://doi.org/10.1016/j.petrol.2019.06.020>

540 Sharma, R., & Srivastava, P. K. (2014). *Hydrothermal Fluids of Magmatic Origin, in Modelling of Magmatic*
541 *and Allied Processes*. Edited by Kumar, S. & Singh, R. N. 181-208, Springer International Publishing, Cham.
542 https://doi.org/10.1007/978-3-319-06471-0_9

543 Siregar, E., Omosanya, K. O., Magee, C., & Johansen, S. E. (2019). Impacts of fault-sill interactions on sill
544 emplacement in the Vøring Basin, Norwegian North Sea. *Journal of Structural Geology*, 126, 156-174.
545 <https://doi.org/10.1016/j.jsg.2019.06.006>

546 Smallwood, J. R., & Maresh, J. (2002). The properties, morphology and distribution of igneous sills:
547 modelling, borehole data and 3D seismic from the Faroe-Shetland area. *Geological Society, London, Special*
548 *Publications*, 197(1), 271-306. <https://doi.org/10.1144/GSL.SP.2002.197.01.11>

549 [Song, X., Li, C., Yao, Y., & Shi, H. \(2017\). Magmatism in the evolution of the South China Sea: Geophysical](#)
550 [characterization. *Marine Geology*, 394, 4-15. <https://doi.org/10.1016/j.margeo.2017.07.021>](#)

551 Subrahmanyam, D., & Rao, P. (2008). *Seismic attributes-A review*. paper presented at 7th international
552 conference & exposition on petroleum geophysics, Hyderabad, India.

553 Sun, Q., Jackson, C. A. L., Magee, C., & Xie, X. (2019). Deeply buried ancient volcanoes control hydrocarbon
554 migration in the South China Sea. *Basin Research*, 32(1), 146-162. <https://doi.org/10.1111/bre.12372>

555 Sun, Q., Alves, T. M., Zhao, M., Sibuet, J.-C., Calvès, G., & Xie, X. (2020a). Post-rift magmatism on the
556 northern South China Sea margin. *GSA Bulletin*, 132(11-12), 2382-2396. <https://doi.org/10.1130/B35471.1>

557 [Sun, Q., Magee, C., Jackson, C. A. L., Mitchell, S. J., & Xie, X. \(2020b\). How do deep-water volcanoes grow?](#)
558 [*Earth and Planetary Science Letters*, 542, 116320. <https://doi.org/10.1016/j.epsl.2020.116320>](#)

559 [Sutherland, R., et al. \(2010\). Lithosphere delamination with foundering of lower crust and mantle caused](#)
560 [permanent subsidence of New Caledonia Trough and transient uplift of Lord Howe Rise during Eocene and](#)
561 [Oligocene initiation of Tonga-Kermadec subduction, western Pacific. *Tectonics*, 29\(2\).](#)
562 <https://doi.org/10.1029/2009TC002476>

563 Svensen, H., Planke, S., Malthe-Sørensen, A., Jamtveit, B., Myklebust, R., Rasmussen Eidem, T., & Rey, S.
564 S. (2004). Release of methane from a volcanic basin as a mechanism for initial Eocene global warming.
565 *Nature*, 429(6991), 542-545. <https://doi.org/10.1038/nature02566>

566 Svensen, H., Jamtveit, B., Planke, S., & Chevallier, L. (2006). Structure and evolution of hydrothermal vent
567 complexes in the Karoo Basin, South Africa. *Journal of the Geological Society*, 163(4), 671-682.
568 <https://doi.org/10.1144/1144-764905-037>

569 Timm, C., Hoernle, K., Van Den Bogaard, P., Bindeman, I., & Weaver, S. (2009). Geochemical Evolution of
570 Intraplate Volcanism at Banks Peninsula, New Zealand: Interaction Between Asthenospheric and Lithospheric
571 Melts. *Journal of Petrology*, 50(6), 989-1023. <https://doi.org/10.1093/petrology/egp029>

572 Tóth, Z., Spiess, V., & Jensen, J. (2014a). Seismo-acoustic signatures of shallow free gas in the Bornholm
573 Basin, Baltic Sea. *Continental Shelf Research*, 88, 228-239. <https://doi.org/10.1016/j.csr.2014.08.007>

574 Tóth, Z., Spiess, V., Mogollón, J. M., & Jensen, J. B. (2014b). Estimating the free gas content in Baltic Sea
575 sediments using compressional wave velocity from marine seismic data. *Journal of Geophysical Research:
576 Solid Earth*, 119(12), 8577-8593. <https://doi.org/10.1002/2014JB010989>

577 Trude, J., Cartwright, J., Davies, R. J., & Smallwood, J. (2003). New technique for dating igneous sills.
578 *Geology*, 31(9), 813-816. <https://doi.org/10.1130/G19559.1>

579 Tulloch, A. J., Ramezani, J., Mortimer, N., Mortensen, J., van den Bogaard, P., & Maas, R. (2009). Cretaceous
580 felsic volcanism in New Zealand and Lord Howe Rise (Zealandia) as a precursor to final Gondwana break-up.
581 *Geological Society, London, Special Publications*, 321(1), 89-118. <https://doi.org/10.1144/SP321.5>

582 van der Meer, Q. H. A., Waight, T. E., Whitehouse, M. J., & Andersen, T. (2017). Age and petrogenetic
583 constraints on the lower glassy ignimbrite of the Mount Somers Volcanic Group, New Zealand. *New Zealand
584 Journal of Geology and Geophysics*, 60(3), 209-219. <https://doi.org/10.1080/00288306.2017.1307232>

585 Velayatham, T., Holford, S. P., & Bunch, M. A. (2018). Ancient fluid flow recorded by remarkably long, buried
586 pockmark trains observed in 3D seismic data, Exmouth Plateau, Northern Carnarvon Basin. *Marine and
587 Petroleum Geology*, 95, 303-313. <https://doi.org/10.1016/j.marpetgeo.2018.05.007>

588 Viskovic, G. P. D. (2010). Investigation of Fluid Migration Pathways in the Shallow Subsurface of the Great
589 South Basin, through the use of High- Resolution Seismic Imaging of Fault and Fracture Systems. MSC thesis.
590 University of Otago.

591 Vlahović, I., Tišljarić, J., Velić, I., & Matičec, D. (2005). Evolution of the Adriatic Carbonate Platform:
592 Palaeogeography, main events and depositional dynamics. *Palaeogeography, Palaeoclimatology,
593 Palaeoecology*, 220(3), 333-360. <https://doi.org/10.1016/j.palaeo.2005.01.011>

594 Wang, L., Sun, Z., Yang, J., Sun, Z., Zhu, J., Zhuo, H., & Stock, J. (2019). Seismic characteristics and
595 evolution of post-rift igneous complexes and hydrothermal vents in the Lingshui sag (Qiongdongnan basin),
596 northwestern South China Sea. *Marine Geology*, 418, 106043. <https://doi.org/10.1016/j.margeo.2019.106043>

597 Zhao, F., Alves, T. M., Wu, S., Li, W., Huuse, M., Mi, L., Sun, Q., & Ma, B. (2016). Prolonged post-rift
598 magmatism on highly extended crust of divergent continental margins (Baiyun Sag, South China Sea). *Earth
599 and Planetary Science Letters*, 445, 79-91. <https://doi.org/10.1016/j.epsl.2016.04.001>

600

601 **Figure Captions**

602 Figure 1. (a) Locations of the Great South Basin (GSB) and the study area (modified from the
603 New Zealand Petroleum and Minerals, 2014). The central edifice (CE; red dashed line), the
604 Tuatara volcanic field (TVF; Phillips & Magee, 2020) and the Papatowai volcanic field (PVF;
605 Bischoff et al., 2020) are marked with; (b) Time-structure map of Horizon T50 (~49 Ma).
606 Locations of mounded structures (M1 - M4) and figures used in this study are labelled.

607 Figure 2. Schematic diagram of the Great South Basin (modified from Killops et al., 1997; Cook
608 et al., 1999; Meadows, 2009). The horizons and locations of wells with radiometric ages are
609 from Bertoni et al. (2019), Sahoo et al. (2022) and Schiøler et al. (2010), respectively. MA:
610 magmatic activities; SDMA: Subduction-related magmatic activities; DIMA: Diffuse intraplate
611 magmatic activities; PRMA: Post-rift magmatic activities; SRMA: Syn-rift magmatic activities.

612 Figure 3. Seismic profile (a) and its interpretation (b). Seismic horizons and main features
613 including the central edifice (CE), mounded structures (M1, M2, M3 and M4), a vertical chaotic
614 zone (VCZ), a depression (D1) and high-amplitude seismic anomalies (AAs) in the study area
615 are labelled. See location in Figure 1.

616 Figure 4. 3D map showing the central edifice (CE), mounded structures (M1-M4), vertical
617 chaotic zone (VCZ) and depression (D1) to display their spatial relationship. Mounded structures
618 M1, 3 and 4 are vertically stacked.

619 Figure 5. (a), (b), (c) and (d) Seismic profiles showing the characteristics of mounded structures
620 (M1, M2, M3 and M4). Onlapping seismic reflections could be identified on the flanks of these
621 mounded structures; (e), (f), (g) and (h) amplitudes envelope of mounded structures; (i), (j), (k)
622 and (l) showing the 3-D shapes of mounded structures. The white dashed lines are the locations
623 of seismic profiles shown in (a)-(h).

624 Figure 6. Seismic profiles (a and d), amplitude envelopes (b and e) and their associated
625 interpretation (c and f) showing the characteristics of mounded structures (M1, M2, M3 and M4),
626 a vertical chaotic zone (VCZ), a depression (D1) and high-amplitude anomalies (AAs). The
627 mounded structures present as conical bodies in the amplitude envelopes, and onlapping seismic
628 reflections are observed at their flanks.

629 Figure 7. Seismic characteristic of the depression (D1) in the study area. (a) and (b) Seismic
630 profiles crossing through the depression. Sediments within the depression onlap onto its flanks;
631 (c) 3-D morphology of the depression; (d) Coherence slice of 2040 ms (TWT: two-way travel
632 time).

633 Figure 8. (a) Seismic profile shown the characteristics of depression (D1) and high-amplitude
634 anomalies (AAs); (b-d) RMS amplitude attributes extracted along the blue dashed line (T70),
635 black dashed line and cyan dashed line (H2) in (a). Seismic amplitude anomalies (AAs) show as
636 high values (warm color).

637 Figure 9. Evolution model of the hydrothermal vents and focused fluid flow system in the study
638 area. (a)-(c) Formation of hydrothermal vents M1 (~75 Ma), M2 (~66 Ma) and M3 (~60 Ma)
639 above the volcanic field; (d) Formation of hydrothermal vent M4 (~56 Ma). M1, M3 and M4
640 shared the same hydrothermal fluid pathway; (e) Fluids firstly accumulated at the peak of
641 hydrothermal vent (M4) and then escaped onto the paleo-seabed to form the pockmark (D1)
642 through the vertical fluid migration pathway (VCZ) in the Early Eocene (~49 Ma); (f) Fluids
643 continued to migrate upward and charged into the strata as young as ~21 Ma (Horizon H2).
644

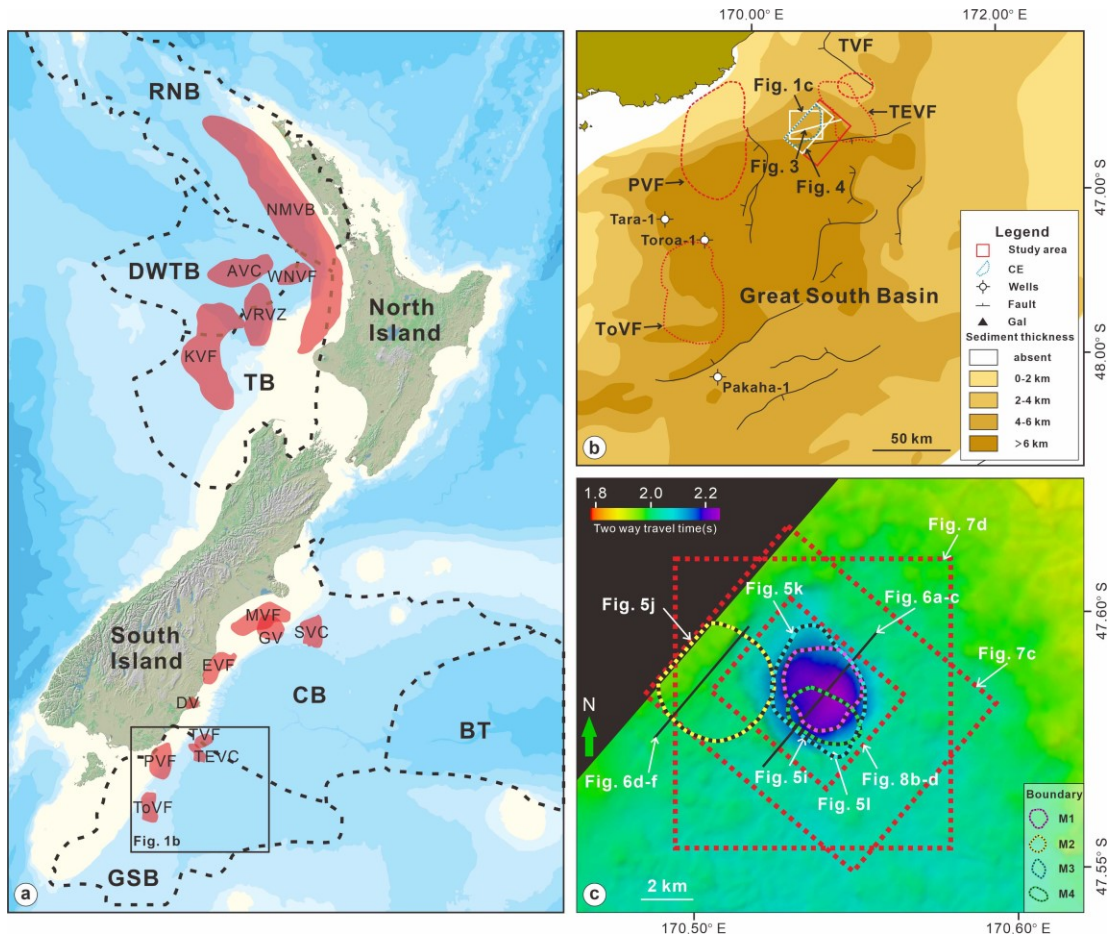


Figure 1. (a) Map showing the region bathymetry of New Zealand and location of offshore volcanoes; (b) Locations of the Great South Basin (GSB) and the study area (modified from the New Zealand Petroleum and Minerals, 2014); (c) Time-structure map of Horizon T50 (~49 Ma). Locations of the central edifice (CE; red dashed line), mounded structures (M1 - M4) and figures used in this study are labelled. RNB: Reinga Northland Basin (XX Ma); DWTB: Deep-water Taranaki Basin; TB: Taranaki Basin; GSB: Great South Basin; CB: Canterbury Basin; BT: Bounty Trough; NWVB: Northland-Mohakatino volcanic belts; AVC: Aotea volcanic complex; WNVF: West Ngatutura volcanic filed; VRVZ: Vulcan-Rommey volcanic belts; KVF: Kaiwero volcanic field; MVF: Maahunui volcanic field; GV: Galleon Volcanics; SVC: Sloop volcanic field; EVF: East Waiareka-Deborah volcanic field; DV: Dunedin volcano; TVF: the Tuatara volcanic field; TEVF: Tapuku East volcanic complex; PVF: the Papatowai volcanic field; ToVF: Toroa volcanic field. (Bischoff et al., 2020; Phillips&Magee, 2020; Tulloch et al., 2009).

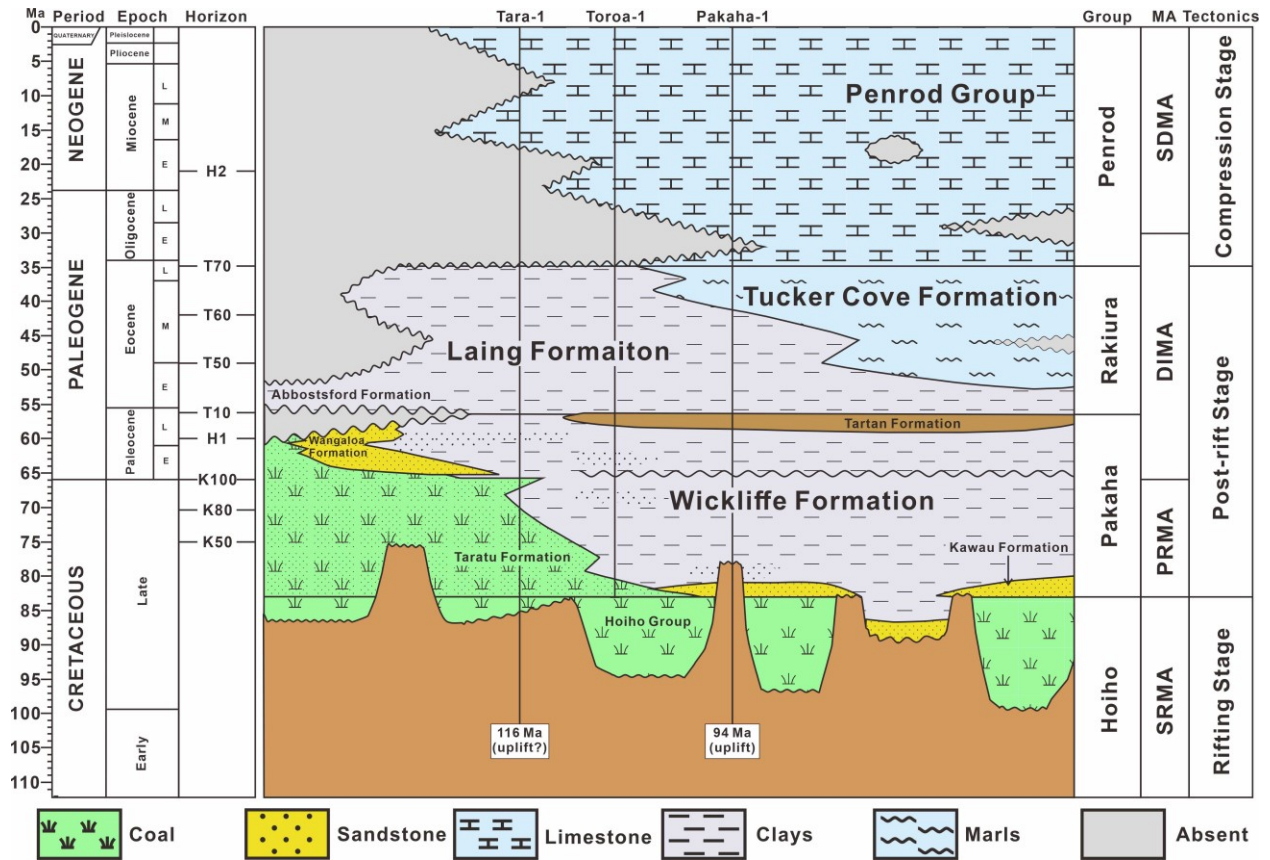


Figure 2. Schematic diagram of the Great South Basin (modified from Killops et al., 1997; Cook et al., 1999; Meadows, 2009). The horizons and locations of wells with radiometric ages are from Bertoni et al. (2019), Sahoo et al. (2022), Schiöler et al. (2010), respectively. MA: magmatic activities; SDMA: Subduction-related magmatic activities; DIMA: Diffuse intraplate magmatic activities; PRMA: Post-rift magmatic activities; SRMA: Syn-rift magmatic activities.

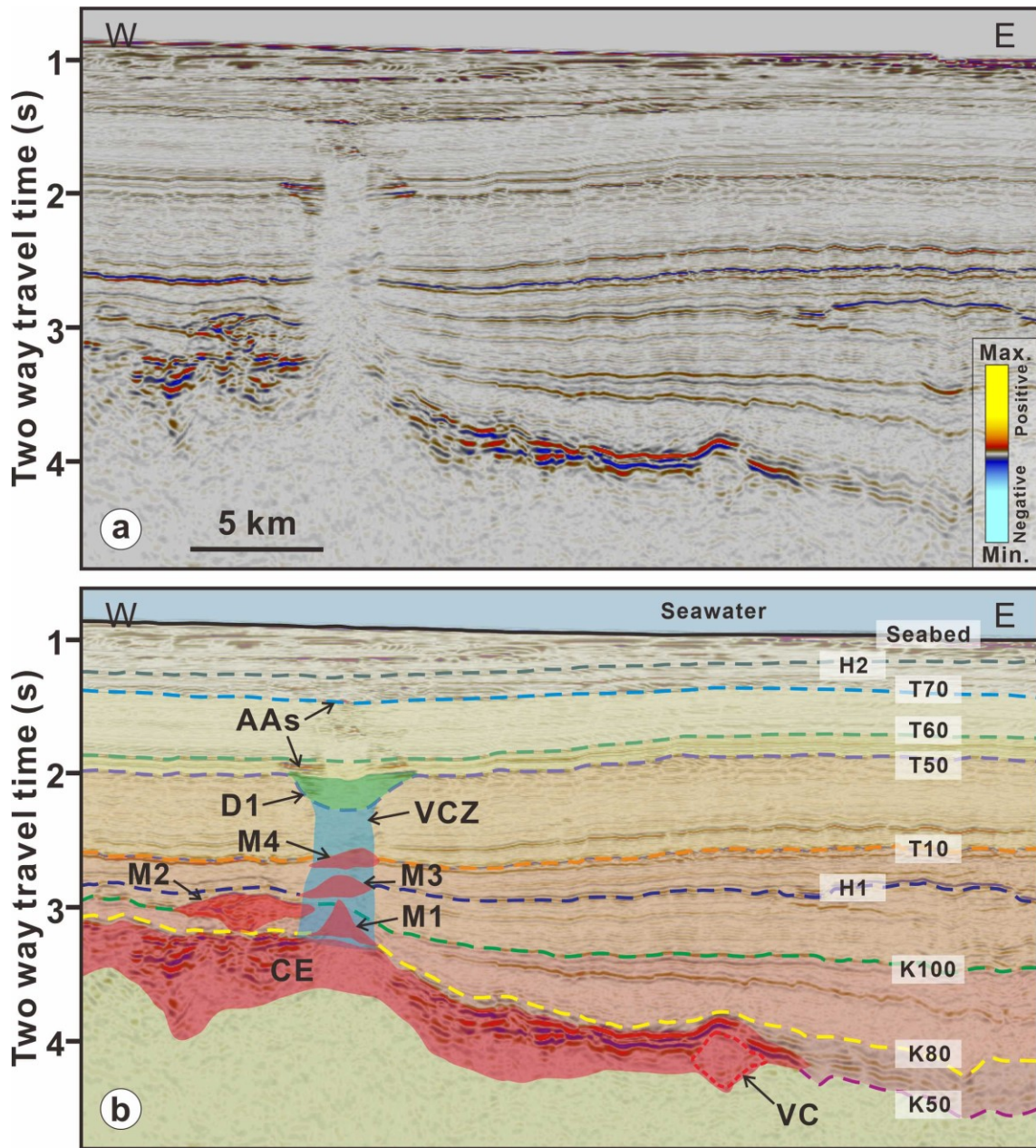


Figure 3. Seismic profile (a) and its interpretation (b). Seismic horizons and main features including the central edifice (CE), volcanic cone (VC), mounded structures (M1, M2, M3 and M4), a vertical chaotic zone (VCZ), a depression (D1) and high amplitude anomalies (AAs) in the study area are labelled. See location in Figure 1.

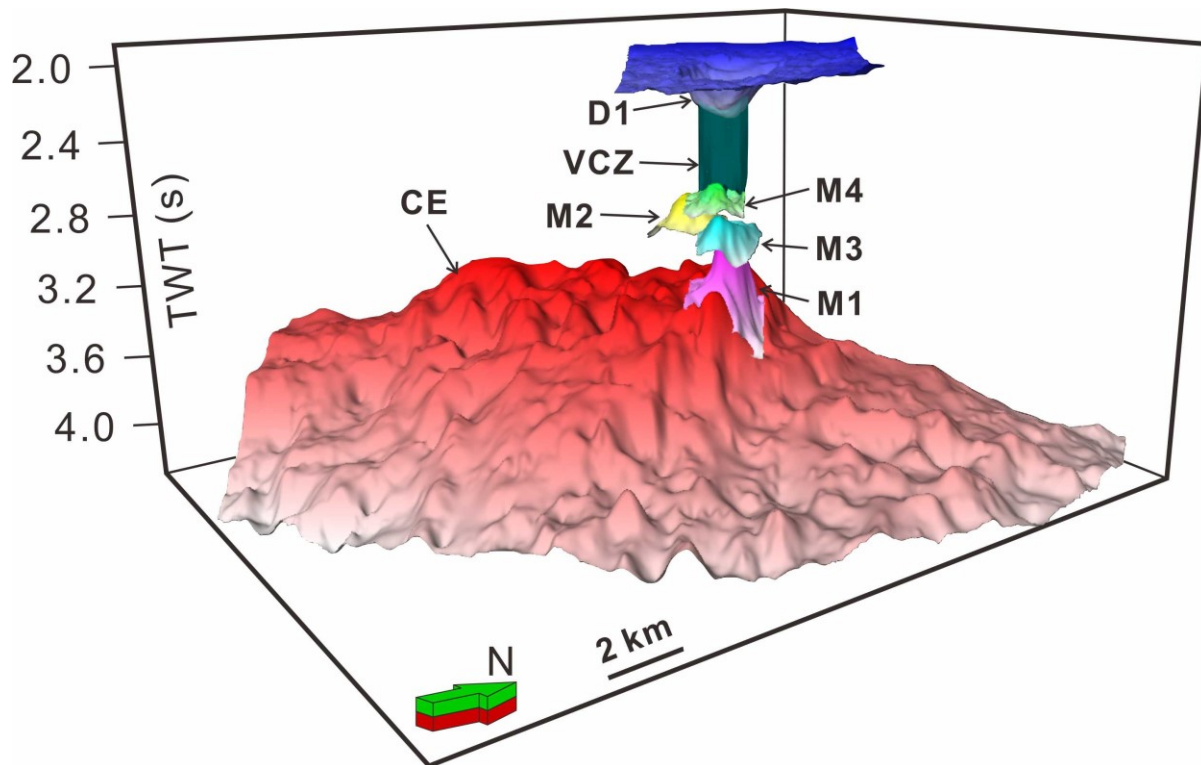


Figure 4. 3D map showing the central edifice (CE) in the study area, mounded structures (M1-M4), vertical chaotic zone (VCZ) and depression (D1) to display their spatial relationship. Mounded structures M1, 3 and 4 are vertically stacked.

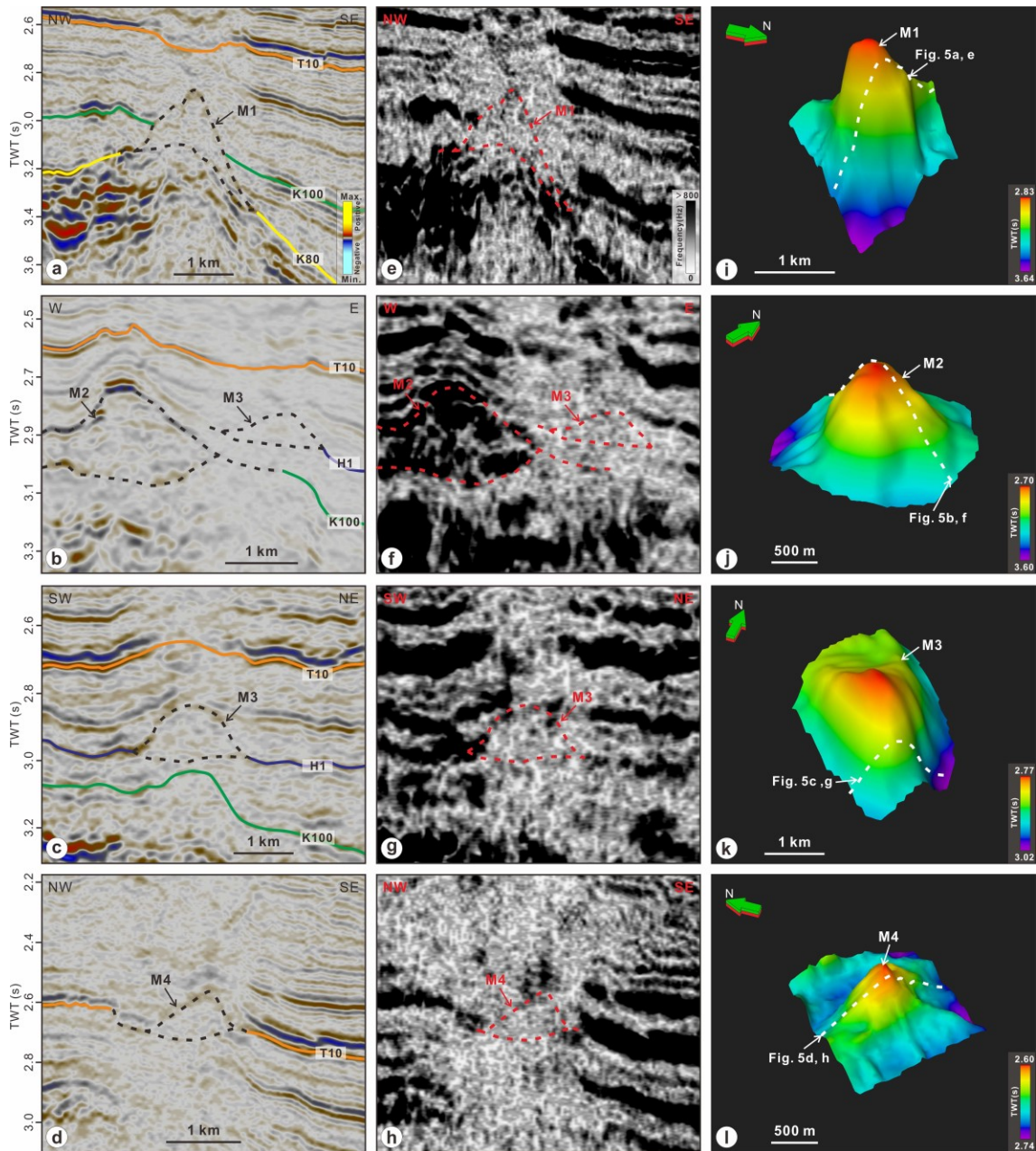


Figure 5. (a), (b), (c) and (d) Seismic sections showing the characteristics of mounded structures (M1, 2, 3 and 4). Onlapping seismic reflections could be identified on the flanks of these mounded structures. (e), (f), (g) and (h) Amplitudes envelope of mounded structures; (i), (j), (k) and (l) Showing the 3-D shapes of mounded structures. The white dashed lines are the locations of seismic sections shown on (a)-(h).

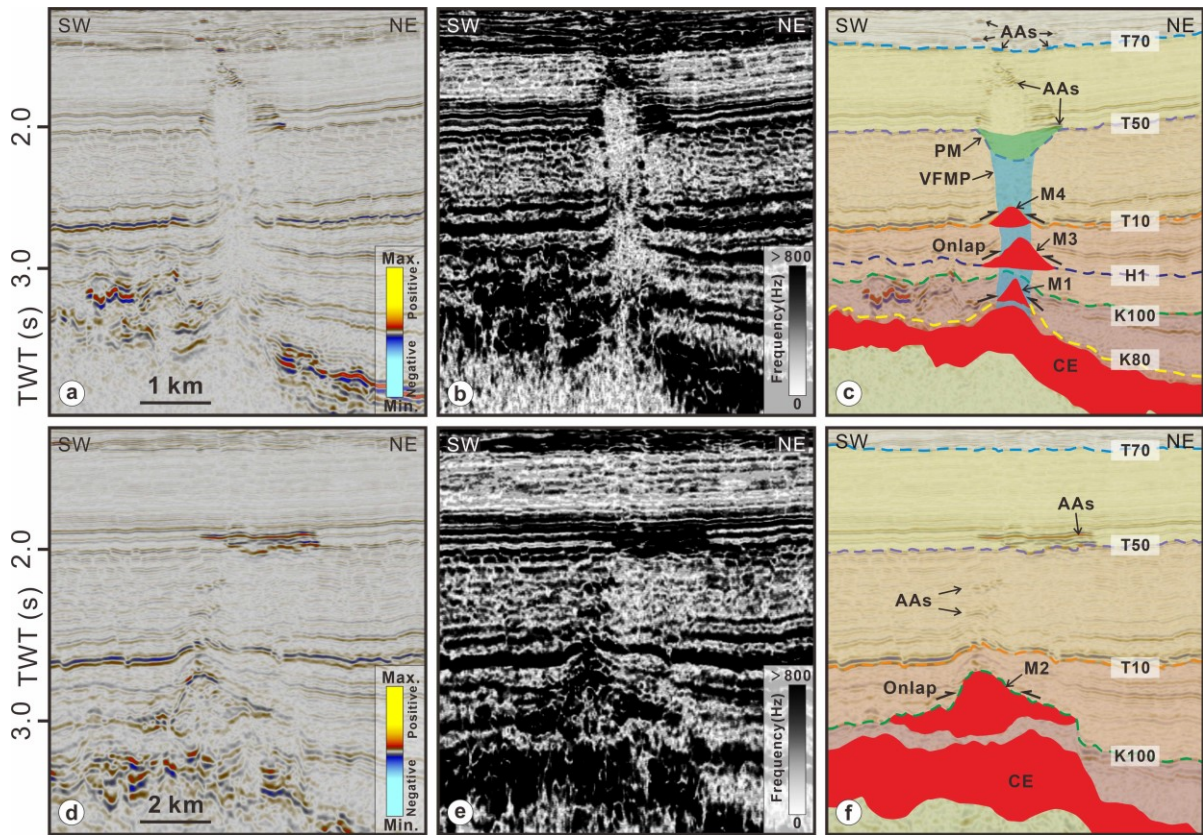


Figure 6. Seismic profiles (**a** and **d**), amplitude envelopes (**b** and **e**) and their associated interpretation (**c** and **f**) showing the characteristics of mounded structures (M1, M2, M3 and M4), a vertical chaotic zone (VCZ), a depression (D1) and high amplitude anomalies (AAs). The mounded structures present as conical bodies in the amplitude envelopes, and onlapping seismic reflections are observed at their flanks.

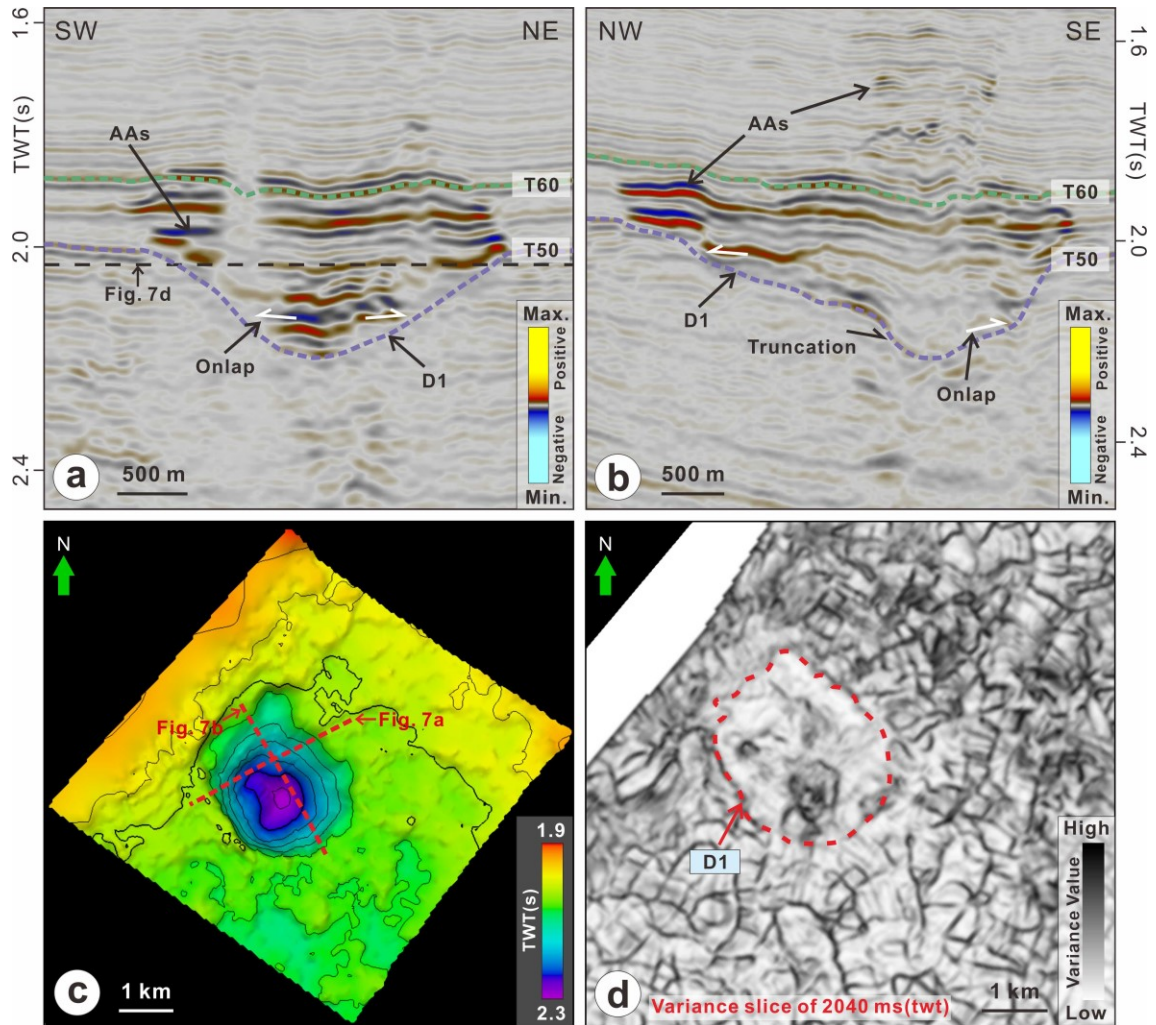


Figure 7. Seismic characteristic of the depression (D1) in the study area. (a) and (b) Seismic profiles crossing through the depression. Sediments within the depression onlapped onto its boundaries; (c) 3-D morphology of the depression; (d) Coherence slices of 2040 ms (tw).

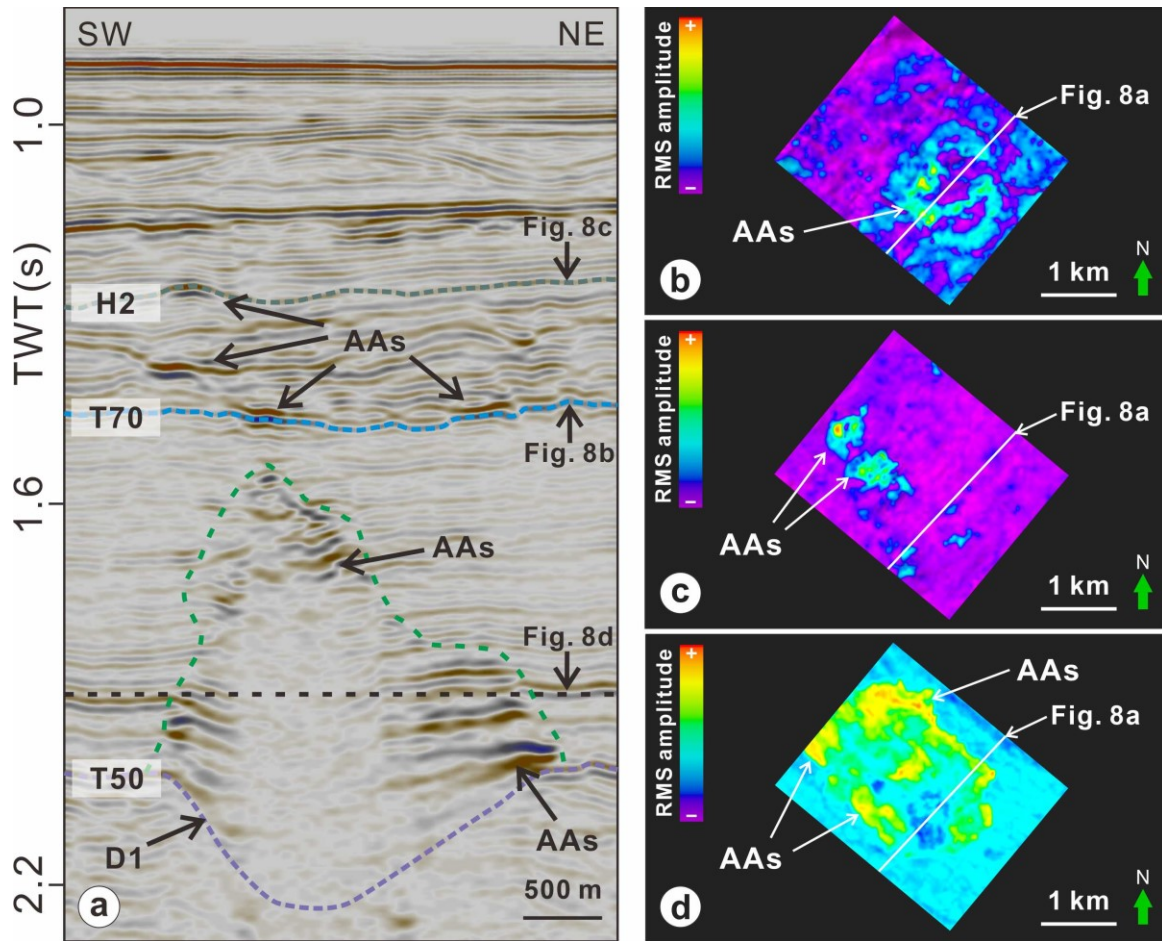


Figure 8. (a) Seismic profile shown the characteristics of depression (D1) and high amplitude anomalies (AAs). (b-d) RMS amplitude attribute extracted along the blue dashed line (T70), black dashed line and cyan dashed line (H2). Seismic amplitude anomalies (AAs) show as high values (warm color)

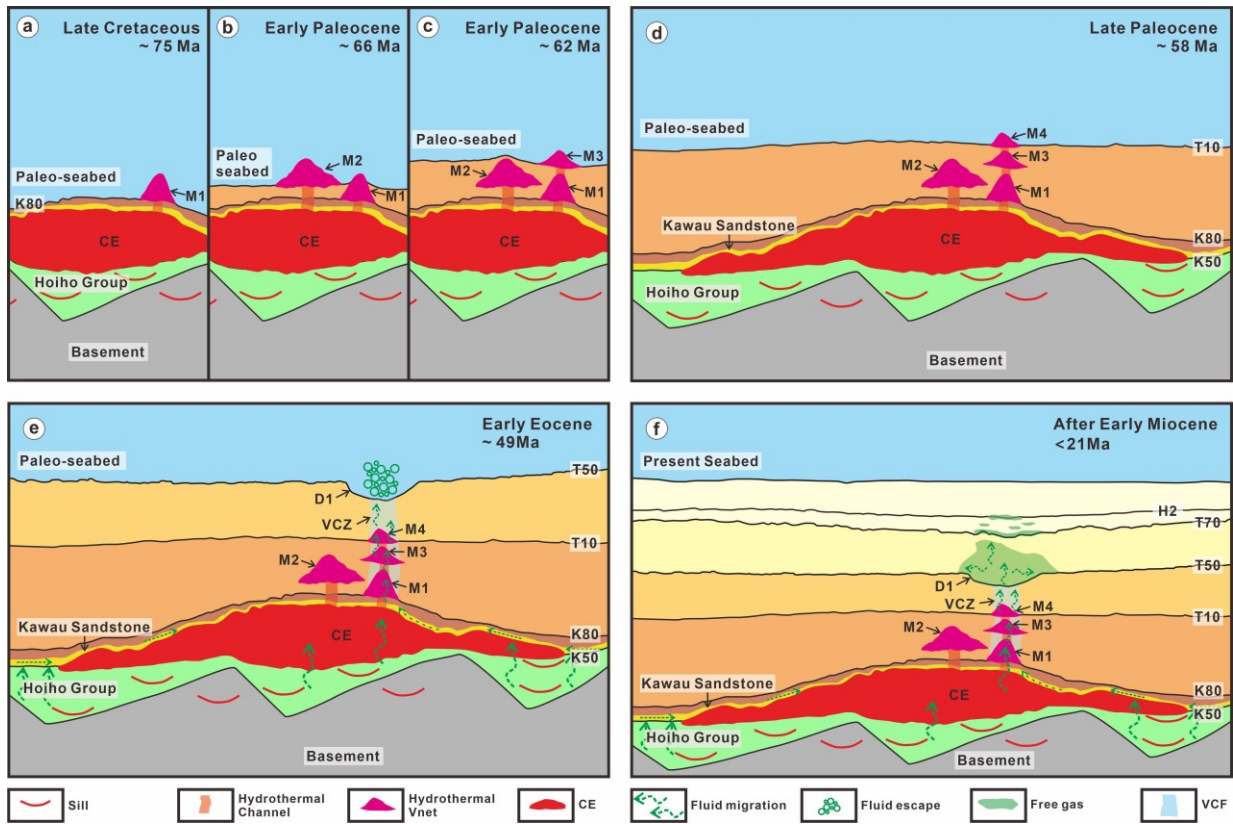


Figure 9. Evolution model of the hydrothermal vents and focused fluid flow system in the study area. (a)-(c) Formation of hydrothermal vents M1 (~75 Ma), M2 (~66 Ma) and M3 (~60 Ma) above the volcanic field; (d) Formation of hydrothermal vent M4 (~56 Ma). M1, M3 and M4 shared the same hydrothermal fluid pathways; (e) Fluids firstly accumulated at the peak of hydrothermal vent (M4) and then escaped onto the paleo-seabed to form the pockmark (D1) through the vertical fluid migration pathway (VCZ) in the Early Eocene (~49 Ma); (f) Fluids continued to migrate upward and charge strata as young as those of Horizon H2 (~21 Ma)